ISSN 2616-5872 Vol.5, Issue 1: 62-70, DOI: 10.25236/AJEE.2023.050109

Geological Hazard Susceptibility Assessment Based on RS and PSO-SVR Model

Ren Dan[a,*], Jia Zhiqiang[b]

College of Earth Science, Guilin University of Technology, Guilin, China
[a]15183791236@163.com, [b]jiazhiqiang@glut.edu.en
**Corresponding author*

Abstract: *It is crucial to undertake thorough study and data mining on factors that determine the occurrence of geohazards to prevent and anticipate their occurrence. A small-sample learning method with a strong theoretical underpinning, the classical support vector machine model provides considerable expressive power in dealing with the interaction of nonlinear characteristics and lessens reliance on the entire data set. However, its excellent generalization capabilities result in an excessively large optimal search space, which impacts the search for kernel parameters and reduces the model's accuracy. The particle swarm algorithm, which has a robust search capability, is thus introduced to improve it. This paper's research area is Chian Town, China. The prediction study of geological hazard susceptibility in Chian town was validated using Gaofen 2 remote sensing imagery in conjunction with a support vector machine regression model enhanced by the particle swarm algorithm. The findings show that the high-risk zone comprises 17% of the overall area and has an 88.88% prediction accuracy. The results imply that integrating high-resolution remote sensing imagery-based and optimized machine learning algorithm models has prospective applications in investigating geological hazard susceptibility with small samples, numerous feature factors, and large-scale data.*

Keywords: *High-resolution remote sensing, PSO-SVR, Geological hazard*

1. Introduction

Geological hazards are events or phenomena that threaten human life, property, or the environment. The pattern of change in its spatial distribution is frequently the result of the interaction of human and natural multi-class elements, subject to the natural environment and human actions. Even though domestic and international scholars have conducted numerous studies in this field [1-11], the complexity and variety of geological and environmental variables make it difficult for accuracy, efficiency, and practicability to coexist. It is crucial to prevent and control geological hazards from a practical aspect to study a more excellent and precise way of prediction. Chian Town, Zhejiang Province, is situated in a hilly coastal region of southeast China. Due to geographical and geological conditions and human engineering activity, geological dangers are common. Using 0.8 resolution Gaofen-2 satellite (GF-2) remote sensing image data, the influencing variables of geological risks in the research region are retrieved and examined in this work. Combining historical geohazard locations, quantifying data, and studying the relationship between various variables and the incidence of geohazards are all components of this research.Based on the river network water system, Chian Town is divided into 44,654 slope units as the evaluation units for this geological hazard susceptibility evaluation. The evaluation units are coupled with quantitative data of various parameters, and the data are normalized using the mapminmax function to get the 44654*N data table. A parameter search for the support vector machine regression model is conducted utilizing the Particle Swarm Optimization algorithm, which may quickly approximate the optimal solution for optimizing system parameters. The trained Particle Swarm Optimization-Support vector machine regression model is then applied to partial data tables for initial training modeling. The geohazard susceptibility index (GSI) is added for validation. Input all data tables into the validated model for the second global test to forecast Chian Town's sensitivity to geological hazards. The geological hazard susceptibility index was calculated for all 44654 slope units in the region. Lastly, the results' correctness was confirmed using the hierarchically graded susceptibility index ratio R and the ROC curve.

ISSN 2616-5872 Vol.5, Issue 1: 62-70, DOI: 10.25236/AJEE.2023.050109

2. Overview of the study area

2.1. Overview of the region

The study area is in Chian Town, Zhejiang Province, China, and is defined by latitude 29°02′12″ 29°10′49″N and longitude 119°53′31″120°05′19″E. The town has a 149.98 square kilometer area. It is located in southeast China's hilly coastline region and is at risk from typhoons and torrential downpours. The region is a part of the South China stratigraphic zone and is situated on the southern side of the Jiang Shao collocation zone. The stratigraphic lithology in the area is diverse and tectonically complex, with the distribution of Cretaceous volcanic rocks, clastic rocks, and a large area of exposed Chen Cai Group gneisses of the Meso-proterozoic Era, with several rock stratigraphic units exposed. The bedrock is widely covered with residual slope deposits, and the vegetation coverage is high. It is densely populated, and artificial excavation of slopes is joint. The overall geomorphology is mainly low hills, with the terrain surrounded by mountains on the north, west, and south and slightly lower in the middle, and the mountain range running northeast. From 1999 to 2020, the area recorded 57 historical disaster sites. 2021 has identified 48 geological hazard sites through remote sensing data interpretation and field verification, mainly located around the foot of the slope of the low hills, on both sides of the highway, and near residential areas.

2.2. Sources of research

This research uses a mix of data collecting and field surveys to get precise data on the geohazard-inducing environment of Chian Town and to ensure the precision of the model prediction. The data sources mainly include: (1)GF-2 satellite remote sensing image two scenes (2021-09-27) for analyzing surface information such as linear structure, water system distribution, human engineering activities, and geological hazard point distribution, show in Figure 1; (2) 30M resolution digital terrain model (Dem) of Chian Town for extracting topographic and geomorphological information such as slope, slope aspect, elevation, and curvature; (3) a Chian Town 1:100000 geological map for extracting geological information such as stratigraphic lithology; and (4) historical geological disaster archives and field survey data for historical geohazard interpretation and spatial positioning.

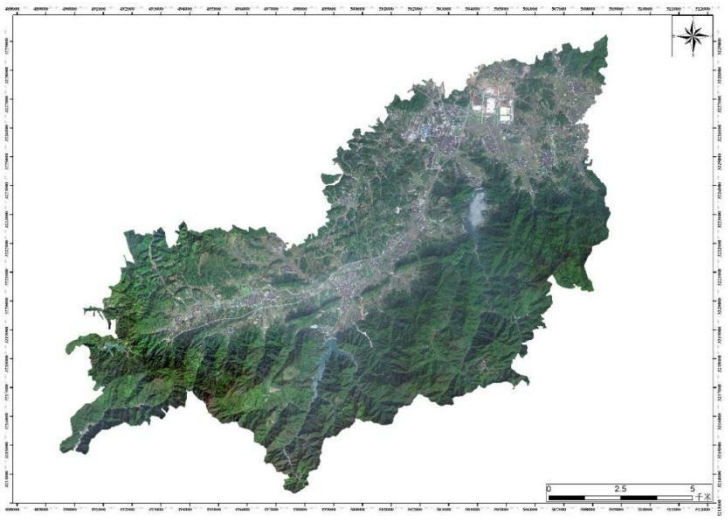

Figure 1: Preprocessed dummy color composite map of a remote sensing satellite image of Chian Town.

2.3. Analysis of the regional geohazards survey

Multiple sources influence the genesis and evolution of geological risks. Based on remote sensing photos of Chian Town, DEM elevation data, geological maps, and geographical analysis of unique regional geological dangers. As influence variables for analyzing the geological hazard susceptibility assessment in Chian Town, the eight categories of the slope, slope aspect, elevation, curvature, stratigraphic lithology, fault, road, and water system were selected and extracted.

To ease quantitative analysis, the eight-factor layers were resampled into 59854 grid cells by 50m*50m and categorized using the natural intermittent point method. The 105 geological disaster points

ISSN 2616-5872 Vol.5, Issue 1: 62-70, DOI: 10.25236/AJEE.2023.050109

were superimposed on each classification of the eight types of variables, and their distribution densities were computed. The correlation analysis table between impact factor classification classes and historical geohazards has been obtained. The association is stronger the larger the ratio's r-value, as shown in Table 1.

Table 1: Correlation analysis of geological hazard impact factors and disasters in Chian Town.

	classify	Grid units	Percentage（A）	Historical geological	Percentage（B）	Ratio r = B/A
slope/（°）	<9	19625	0.327881178	22	0.209524	0.639024
	9-22	9386	0.156814916	19	0.180952	1.153923
	22-33	13730	0.229391519	29	0.276190	1.204013
	33-43	11829	0.197630902	26	0.247619	1.252937
	43-71	5284	0.088281485	9	0.085714	0.970920
Aspect	plane	16569	0.276823604	20	0.190476	0.688078
	N	5515	0.092140876	9	0.085714	0.930253
	NE	6181	0.103267952	10	0.095238	0.922243
	E	5490	0.091723193	12	0.114286	1.245985
	SE	5369	0.089701607	16	0.152381	1.698754
	S	4021	0.067180138	13	0.123810	1.842948
	SW	4774	0.079760751	7	0.066667	0.835833
	W	5457	0.091171852	12	0.114286	1.253520
	NW	6478	0.108230026	6	0.057143	0.527976
Elevation/m	65-169	24797	0.414291443	21	0.200000	0.482752
	169-298	9237	0.154325525	42	0.400000	2.591924
	298-435	10374	0.17332175	29	0.276190	1.593513
	435-578	10098	0.168710529	12	0.114286	0.677407
	578-915	5348	0.089350754	1	0.009524	0.106589
curvature	-494--28	806	0.013466101	2	0.019048	1.414487
	-28--7	4861	0.081214288	20	0.190476	2.345353
	-7-5	47443	0.792645437	73	0.695238	0.877111
	5-23	5853	0.097787951	8	0.076190	0.779140
	23-609	891	0.014886223	2	0.019048	1.279547
Stratigraphic lithology	Xishantou group	10390	0.173589067	28	0.266667	1.536195
	Yinjinagqiao group	5527	0.092341364	2	0.019048	0.206274
	Chaochuan group	5528	0.092358071	0	0.000000	0.000000
	Gaowu group	12965	0.216610419	27	0.257143	1.187121
	Dashuang group	10868	0.181575166	21	0.200000	1.101472
	Chencai group	14576	0.243525913	27	0.257143	1.055916
fault（distance）/m	<50	3492	0.058341965	9	0.085714	1.469170
	50-100	3548	0.059277575	14	0.133333	2.249305
	100-150	3488	0.058275136	16	0.152381	2.614854
	150-200	3496	0.058408795	12	0.114286	1.956653
	>200	45830	0.765696528	54	0.514286	0.671657
road（distance）/m	<25	9712	0.162261503	51	0.485714	2.993404
	25-50	7121	0.118972834	14	0.133333	1.120704
	50-75	6030	0.100745147	14	0.133333	1.323472
	75-100	5235	0.087462826	7	0.066667	0.762229
	>100	31756	0.53055769	19	0.180952	0.341061
Water System（distance）/m	<50	9024	0.150766866	14	0.133333	0.884368
	50-100	7861	0.131336252	10	0.095238	0.725147
	100-150	6509	0.108747953	7	0.066667	0.613038
	150-200	5005	0.083620142	9	0.085714	1.025044
	>200	31455	0.525528787	65	0.619048	1.177952

Among these, (1) slope, slope aspect, and slope curvature are crucial elements influencing slope stability. 91% of the geohazards occur on gently sloping slopes below 43°, and the accumulation of residual slope deposits in this area provides rich material sources for the occurrence of geohazards. The geological hazards show a gradually increasing trend from E, SE, and S in the slope direction ratio and

ISSN 2616-5872 Vol.5, Issue 1: 62-70, DOI: 10.25236/AJEE.2023.050109

reach 1.8 in the S ratio. The eastern typhoon and solar radiation illumination strongly influence this partition. The curvature indicates the complexity of the terrain. The curvature values >0 are classified as convex slopes, <0 are classified as concave slopes, and it can be seen that 90% of the geological hazards occur on open slopes. The rate of landslide occurrence in this area of curvature from-28 to-7 reaches 2.3. (2) Geologic elevation influences the scope of human activities, mound distribution, and vegetation. 88% of the geologic hazards are located below 435m, among which the rate is close to 2.6 in the classification area of 169~298. (3) The stratigraphic lithology affects the material basis of disaster development. The Xitoushan Group, Gaowu Group, and Dashuang Group, with a ratio greater than 1, are dominated by tuffs, which are complex and dense and have a solid overall resistance to weathering, making it easy to form high and steep hills. While the Chennai Group Formation of the Meso-proterozoic Erathem, with a ratio of 1, is dominated by gneisses with weak weathering resistance, fissure development, and large thickness of weathered layers. (4) Tectonic conditions are a significant constraint to the occurrence of geological hazards, and the ratio within 200 meters of the fault is greater than 1. (5) Road slope-cutting works are the primary type of mountainous geological hazards induced by human activities. 50% of the geological hazard points are distributed within 25m of the road, corresponding to a ratio of 3, reaching the highest value of 8 types of evaluation factors classification ratio. (6) In the distance range of 150 m from the water system, the ratio shows a trend of gradually decreasing with increasing distance, which indicates that the surface water system has a specific hollowing effect on the slope angle and makes it less stable.

The above analysis demonstrates that the eight influencing factors have a high correlation with the geological dangers of Chian Town. Simultaneously, all elements are interconnected and need to be considered comprehensively in practical prediction. Therefore, we inputted the aforementioned eight indicative factors into the PSO-SVR model with strong learning generalization capacity and good "robustness." to analyze the susceptibility of geohazards.

3. Prediction and validation of PSO-SVR-based geohazard susceptibility evaluation

3.1. Evaluation unit division

The evaluation unit is the smallest spatial map element for geological hazard susceptibility evaluation, and its unit can be a regular or irregular map element [12]. Considering that the development stages of rivers and valleys have an apparent integrated control on the conditions of geological hazard formation [13]. This paper used the slope units of the ridge and river network division based on GIS data to evaluate this prediction. The unreasonable units were checked and modified by manual visual inspection. Finally, 98 slope units containing 105 historical geological hazard points and 44,556 general slope units were obtained. The extracted eight types of evaluation factors corresponding to the conditional attributes were combined with 44,654 slope units. The initial data set of 44556 rows*8 columns is formed.

3.2. PSO-SVR Principle

3.2.1. Support vector machine model

Support vector machine model [14,15](SVM) is a machine learning method based on statistical learning theory, VC dimensional theory, and the structural risk minimization principle, which was first proposed by Vapink et al. in 1995 [16]. The core idea is to transform the sample into a high-dimensional feature space by selecting a kernel function to solve a convex quadratic optimization problem to ensure that the extreme value solution found is the optimal global solution. A small number of small samples determine the final decision. The kernel parameter g, which transfers the samples from one dimension to an unlimited number of dimensions, and the search speed for the penalty parameter c, which controls the training speed and precision, are the determinants of the search for the optimal hyperplane. However, the conventional support vector machine only provides algorithms for two-class classification. In contrast, the classification problem of many classes is typically resolved through data mining for real-world applications of geohazard prediction. As a result, the branch of support vector machines utilized for regression prediction will be used in this work. The great generalizability of the support vector machine regression model (SVR). However, the robust generalization capability of SVR results in an excessively large optimal search space, which makes the model susceptible to prematurely interpreting the local optimum as the global optimum. To improve the support vector machine regression model, the PSO algorithm's robust global search capability was introduced.

ISSN 2616-5872 Vol.5, Issue 1: 62-70, DOI: 10.25236/AJEE.2023.050109

3.2.2. Particle swarm optimization algorithm

The Particle Swarm Optimization (PSO) algorithm is a computational method for global optimization based on population intelligence that Kennedy and RCEberhart proposed in 1995. It was inspired by the simulation of bird predation behavior [17,18]. In an iteration, the particles update themselves by following two optimal solutions: the individual particle extremum best and the particle population extremum best. The approach is widely utilized in function optimization [19,20]because of its rapid convergence, few parameters, and straightforward implementation. In this research, we will use the robust global search capacity of PSO to search for the optimal kernel parameter g and penalty parameter c of the SVR model to practice the usefulness of the optimizing machine algorithm model in forecasting the susceptibility of geohazards.

3.3. Prediction of the PSO-SVR model

3.3.1. Configuring the PSO algorithm initialization parameters[21,22], as shown in Table 2.

Table 2: Initial PSO-SVR algorithm parameter settings.

pso_option.maxgen	50
pso_option.sizepop	20
pso_option.v	5
pso_option.c1	1.2
pso_option.c2	1.2
pso_option.wV	0.9
pso_option.k	1/10
pso_option.cbound	[0.001,100]
pso_option.gbound	[0.001,1000]

Based on parameters such as the number of iterations and population size, the optimal kernel parameter g and penalty parameter c for the SVR model was determined to be Bestg=0.067013 and Bestc=15,1117, as shown in Figure 2. The average fitness value shows the goodness and convergence of the entire population. In contrast, the proximity of the average fitness curve to the optimal fitness curve indicates how near each individual is to the optimal solution.

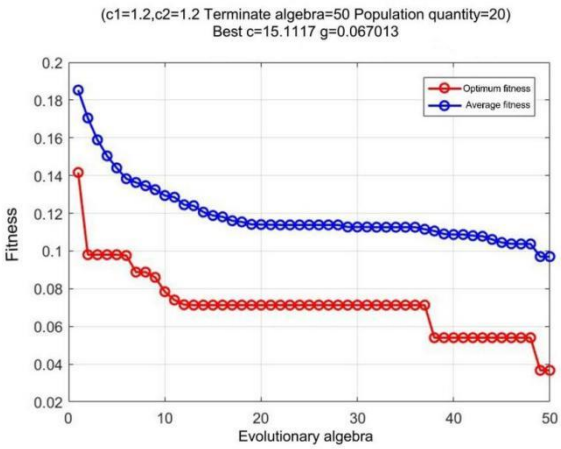

Figure 2: Graph of the adaptation curve (PSO method).

3.3.2. SVR model training and testing

To reduce the effect of the difference in values of the eight types of evaluation factors, the mapminmax function was used to normalize the values to the interval from 0 to 1. From the initial data set, 130 slope cells were extracted and utilized as input for the first test of the POS-SVR model. This includes 98 slope cells containing 105 known hazards and 32 normal slope cells. 80% are selected randomly as training data for the model, while the remaining 20% are utilized as accuracy check samples. Set the value of the geohazard Susceptibility Index (GSI) between 0 and 1, which served as the output for training and validating the SVR model. Figure 3 depicts the training outcomes of the predicted values versus the expected values.

ISSN 2616-5872 Vol.5, Issue 1: 62-70, DOI: 10.25236/AJEE.2023.050109

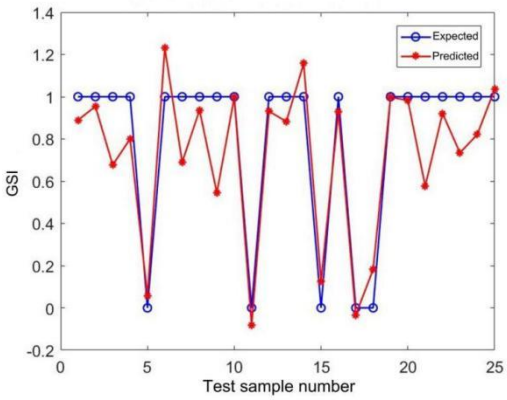

Figure 3: Comparison of predicted and expected values of the PSO-SVR model test set.

The prediction results showed that the maximum value of GSI was 1.2306, and the minimum value was 0.5445 for a sample of 98 slope cells containing known historical hazards. The maximum value of GSI was 0.1813, and the minimum value was-0.0808 for an example of 32 normal slope cells. This finding suggests that the POS-SVR model, based on the combination of Bestg = 0.067013 and Bestc = 15.1117is reasonably practicable for assessing the susceptibility of Chian Town to geological hazards.

3.3.3. Prediction of Chian Town's geological hazard susceptibility

Based on the established PSO-SVR model and input of the complete initial data set, a second training was performed on a sample of 44,564 slope units in the Chian Town area. After one-by-one prediction, the GSI values for each slope unit were acquired. The minimum value is -0.2015, and the maximum value is 1.4121. To visualize the degree of geohazard susceptibility of each point in the region, all the GSI values of slope units are converted to the remote sensing data map of Chian Town. According to the principle of equal distance, the normalized GSI values are split into five regional groups: low, lower, medium, higher, and high geohazard susceptibility. The geological hazard susceptibility rating map for Chian Town was acquired (see Figure 4).

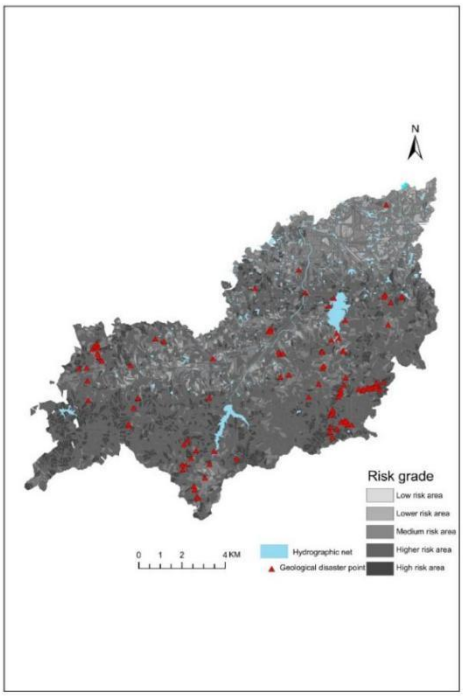

Figure 4: Geological hazard susceptibility grading chart for Chian Town.

To differentiate the degree of geological hazard susceptibility among the five region classes and assess

ISSN 2616-5872 Vol.5, Issue 1: 62-70, DOI: 10.25236/AJEE.2023.050109

the evaluation results' validity. The area of different susceptibility areas A/m2 as determined by statistics; the ratio AR% of the total area of Chian Town (excluding the water area) corresponding to this area; the number of historical geohazard points distributed in each of the five regions B; and the ratio BR% of the geohazard points contained in each area to the total historical geohazard points. Lastly, the hierarchically graded susceptibility index ratio R(R=BR/AR) of geological risks occurring in each class zone's units is calculated. The greater the R-value, the greater the susceptibility to geological hazards. See Table 3.

The R-values of the low, low, and medium susceptibility regions exhibit a little upward trend, whereas the total value is low (less than 0.545). In contrast, the R-values of the high and high susceptibility regions grow significantly from the preceding level, reaching a maximum of 1.8266. This demonstrates that the PSO-SVR-based forecast of geological hazards in Chian Town is reasonable and accurate.

Table3: PSO-SVR model geological hazard susceptibility evaluation grading prediction results.

Risk grade	A/m²	AR%	B	BR%	R=BR/AR
Low risk area	69465.7991	0.0005	0	0.0000	0.0000
Lower risk area	10974081.6797	0.0741	3	0.0286	0.3855
Medium risk area	38809718.9711	0.2621	15	0.1429	0.5450
Higher risk area	72734921.1849	0.4912	54	0.5143	1.0469
High risk area	25476780.8606	0.1721	33	0.3143	1.8266

3.4. Prediction of the PSO-SVR model

To further quantitatively evaluate the accuracy of the PSO-SVR model, the Receiver Operating Characteristic (ROC)[23,24] curve was introduced here. Chian Town's absolute cumulative frequency (percent) of geohazard occurrence-GSI (percent) curve was plotted by dividing the GSI value into 100 equal horizontal coordinates and replacing the actual distribution of known historical geohazard sites as vertical coordinates (Figure 5). The area of the entire mapped area is regarded to be 1.0, and the closer the Area Under Curve (AUC)[23] is to this number, the more accurate the forecast is portrayed. Figure 5's AUC = 0.8888 indicates that the accuracy of the prediction is 88.88%.

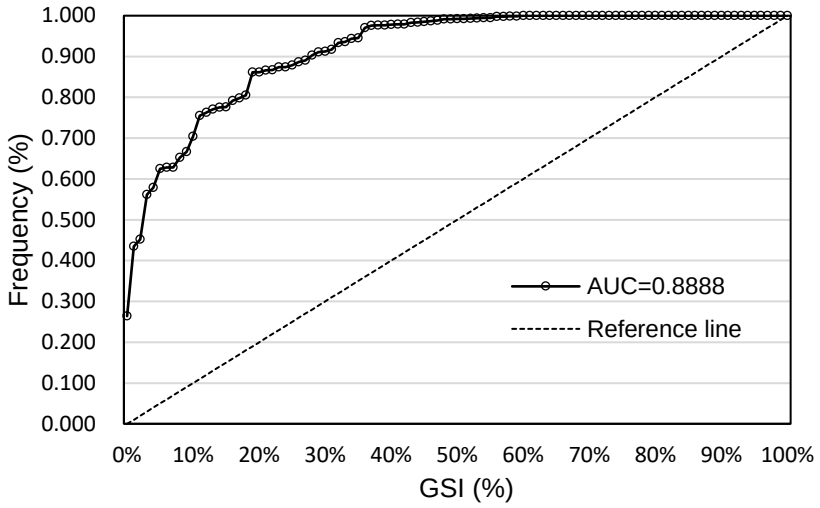

Figure 5: Actual cumulative frequency of geological hazards (%)-(GSI) (%) Graph.

4. Conclusion

4.1. Evaluation unit division

Based on high-resolution remote sensing images, multi-source historical data, and optimized trained intelligent algorithms, this paper conducted a large-scale, high-precision, and high-time-effective study on the geological hazard susceptibility of Chian Town; Eight evaluation factors of geological hazard

ISSN 2616-5872 Vol.5, Issue 1: 62-70, DOI: 10.25236/AJEE.2023.050109

susceptibility were extracted, and two evaluation units were used. It includes the quantitative analysis of the correlation and importance of the extracted influence factors by using the easy-to-calculate grid units and the prediction of the susceptibility by using the slope unit input model, which is closely related to the geological, environmental conditions based on the above work, the susceptibility evaluation of the geological risks in Chian Town has been finished.

This study yielded the following tentative understanding:

The advantages of high-resolution remote sensing images in terms of high accuracy, timeliness, and comprehensive coverage can effectively overcome the disadvantages of a time-consuming and limited range of traditional field exploration methods, and their data selection rationality and numerical accuracy have promising practical applications in the precise prevention of regional geological hazards.

With a full global search capacity, the POS optimization algorithm enables a quick search for the ideal SVR parameters. It allows the PSO-SVR model to demonstrate powerful learning and generalization capabilities in the integrated handling of complex, diverse, and highly correlated geohazard impact factors as well as small samples (97 slope cells containing known historical geohazards) with a large prediction volume (44,556 slope cells of unknown susceptibility).

Geological risks originate and evolve as a result of the interaction of numerous contributing variables. The R-value of the correlation analysis indicates that topography and geomorphology, geological structure, and human engineering activities are the three main categories, among which artificial slope cutting due to road construction is the main triggering factor of geological hazards.

The emergence of geological risks is a complicated process. Although a high level of prediction accuracy was achieved in this study, there are still certain issues that require additional investigation: ① The applicability of the PSO-SVR model to a larger study region. ② Extraction of the respective effect factors for various regional situations. ③ The feasibility of multi-class optimization algorithms for optimizing the accuracy of the SVR model.

References

[1] BA. Akgun et al., "An easy-to-use MATLAB program (MamLand) for the assessment of landslide susceptibility using a Mamdani fuzzy algorithm [J]." Computers & Geosciences. 38(1):23-34(2012) doi.org/10.1016/j.cageo. 2011.04.012

[2] Wang Shang-qing et al., "Early warning method of landslide danger in Baishui River of Three Gorges Reservoir [J]." Journal of Wuhan University (Information Science Edition).34(10):1218-1221(2009)

[3] He Manchao. "Remote monitoring and forecasting system for landslide geological hazards and its engineering application[J]." Journal of Rock Mechanics and Engineering.28(06):1081-1090(2009)

[4] J, Mathew, et al., "Landslide susceptibility zonation mapping and its validation in part of Garhwal Lesser Himalaya, India, using binary logistic regression analysis and receiver operating characteristic curve method[J]." Landslides. 6(1): 17-26. DOI: 10.1007/s10346-008-0138-z (2009) doi.org/10.1007/s 10346-008-0138-z

[5] E.A. Sezer, et al., "Manifestation of an adaptive neuro-fuzzy model on landslide susceptibility mapping: Klang valley, Malaysia[J]." Expert Systems with Application. 38(7):8208-8219(2011) doi.org/10.1016/j.eswa.2010.12.167

[6] B.Pradhan, "Approaches for Delineating Landslide Hazard Areas Using Different Training Sites in an Advanced Artificial Neural Network Model[J]." Journal of Geospatial Information Science. 13(2): 93-102. doi.org/10.1007/s11806-010-0236-7

[7] ZHANG Baolei, "Investigation and Assessment of Landslides and Debris Flows in Sichuan Province of China by Remote Sensing Technique[J]." China Geoscience. 16(3):223-228(2006)doi.org/10.1007/ s11769-006-0223-y

[8] Yu Bu et al., "Geological hazard zoning and evaluation of landslide hazard in Hangzhou[J]." Geotechnics.33(S1):193-199+216. 10.16285/j.rsm.2012.s1.007

[9] R, Samanef et al. "Mapping landslide susceptibility with frequency ratio, statistical index, and weights of evidence models: a case study in northern Iran[J]." Environmental earth sciences. 76(14) (2017) doi.org/10.1007/s12665-017-6839-7

[10] Hu Yan et al., "Evaluation of landslide hazard susceptibility in Badong County based on the right-of-evidence method[J]." Geological Science and Technology Bulletin.39(03):187-194(2020) 10.19509/j. cnki.dzkq.2020.0320.

[11] A.D. Regmi et al., "Application of frequency ratio, statistical index, and weights-of-evidence models

ISSN 2616-5872 Vol.5, Issue 1: 62-70, DOI: 10.25236/AJEE.2023.050109

and their comparison in landslide susceptibility mapping in Central Nepal Himalaya[J]." Arabian journal of geosciences. 7(2):725-742(2014) doi.org/10.1007/s12517-012-0807-z

[12] Tian Shu-jun et al., "Comparative study of landslide susceptibility evaluation based on different evaluation units[J]." Journal of Natural Hazards. 28(06):137-145(2019) 10.13577/j.jnd.2019.0615

[13] Huo Ai-di et al., "The method of dividing geological hazard susceptibility evaluation units--an example of Huangling County, Shaanxi Province"[J]. Journal of Jilin University (Earth Science Edition). 41(02):523-528+535(2011) 10.3969/j.issn.1671-5888.2011.02.027

[14] T-Zhang. "An Introduction to Support Vector Machines and Other Kernel-Based Learning Methods[J]." AI magazine: Artificial intelligence. 22(2):103-104(2001)

[15] Z, Xue-gong. "On statistical learning theory and support vector machines[J]." Journal of Automation. 01:36-46(2000) 10.16383/j.aas.2000.01.005.

[16] Vapink V. "Nature of Statistical Learning Theory[M]."New York: Wiley(1995) doi.org/10.1007 /978-1-4757-2440-0

[17] J. Kennedy, R. Eberhart. "Particle swarm optimization[C]." Neural Networks, 1995. Proceedings., IEEE International Conference on vol.4. pp. 1942-1948, Perth, Australia (1995)

[18] Y. Shi, R.C. Eberhart. INSTITUTE OF ELECTRIC AND ELECTRONIC ENGINEER. "Empirical study of particle swarm optimization[C]." //Evolutionary Computation, 1999. CEC 99. Proceedings of the 1999 Congress on Vol. 3. pp. 1945-1950, DC, USA (1999)

[19] Li QING et al., "An improved ant colony algorithm based on particle swarm parameter optimization[J]." Control and Decision Making. 28(06):873-878+883(2013) 10.13195/j.cd.2013.06. 75.liq.016.

[20] Yi-Tung Kao, et al., "A hybrid genetic algorithm and particle swarm optimization for multimodal functions [J]." Applied Soft Computing. 8(2):849-857(2008) doi.org/10.1016/j.asoc.2007.07.002

[21] I.C. Trelea. "The particle swarm optimization algorithm: convergence analysis and parameter selection [J]." Information processing letters. 85(6):317-325(2003) doi.org/10.1016/S0020-0190(02) 00447-7

[22] L.Zhi-xiong et al., "Setting and experimental analysis of random number parameters in particle swarm algorithm[J]." Control Theory and Applications. 27(11):1489-1496(2010)

[23] AP. Bradley. "The Use Of The Area Under The Roc Curve In The Evaluation Of Machine Learning Algorithms [J]. " Pattern Recognition: The Journal of the Pattern Recognition Society. 30(7):1145-1159(1997) doi.org/10.1016/S0031- 3203(96)00142-2

[24] F.TOM. "An introduction to ROC analysis [J]." Pattern recognition letters. 27(8):861-874(2006) doi.org/10.1016/j.patrec.2005.10.010